

Towards a Configuration-space Interaction with the Quantum Potential as its Continuum limit: Part I

Xabier Oianguren-Asua

Abstract— In this first part of the study, we introduce the problem, the implemented software for its analysis and the results of an initial exploratory computational search for a configuration-space force between classical mechanics Universes, that has the quantum potential characterizing the Schrödinger equation as its continuum limit.

1 A CONTINUUM OF CLASSICAL UNIVERSES

As an introduction, let us root the objectives of the work in theoretical grounds. Consider a non-relativistic isolated system of $n \in \mathbb{N}$ degrees of freedom $\vec{x} = (x_1, \dots, x_n) \in \mathbb{R}^n$, e.g. the system of all the particles in the Universe¹. According to the quantum theory, the state of a system in each time t is given by the complex wavefunction $\psi(\vec{x}, t)$, the dynamics of which is given by the Schrödinger Equation (SE),

$$i\hbar \frac{\partial \psi(\vec{x}, t)}{\partial t} = \sum_{k=1}^n \frac{-\hbar^2}{2m_k} \frac{\partial^2 \psi(\vec{x}, t)}{\partial x_k^2} + V(\vec{x})\psi(\vec{x}, t), \quad (1)$$

where m_k is the mass linked to the k -th degree of freedom, \hbar is the so-called Planck constant and $V(\vec{x})$ is the potential energy describing the interactions between the degrees of freedom².

Let us denote by $S(\vec{x}, t)$ and $\rho(\vec{x}, t)$ the wavefunction's phase and magnitude squared, respectively (the last being related to the probability density of finding the system at a configuration \vec{x}). Then, using the polar form $\psi(\vec{x}, t) = \rho^{1/2}(\vec{x}, t)\exp(iS(\vec{x}, t)/\hbar)$, the SE decouples into two real partial differential equations,

$$\frac{\partial \rho(\vec{x}, t)}{\partial t} = - \sum_{k=1}^n \frac{\partial}{\partial x_k} \left[\rho(\vec{x}, t) v_k(\vec{x}, t) \right], \quad (2)$$

$$-\frac{\partial S(\vec{x}, t)}{\partial t} = \sum_{k=1}^n \frac{1}{2} m_k v_k(\vec{x}, t)^2 + V(\vec{x}, t) + Q(\vec{x}, t), \quad (3)$$

where we defined the fields

$$v_k(\vec{x}, t) := \frac{1}{m_k} \frac{\partial S(\vec{x}, t)}{\partial x_k}, \quad (4)$$

$$Q(\vec{x}, t) := -\frac{\hbar^2}{4m_k} \left(\frac{1}{\rho} \sum_k \frac{\partial^2 \rho}{\partial x_k^2} + \frac{1}{2\rho^2} \sum_k (\frac{\partial \rho}{\partial x_k})^2 \right). \quad (5)$$

If we interpreted v_k as the velocity field of the k -th degree of freedom, and therefore following classical mechanics, S was the action, the two partial differential equations (2) and (3), would be nothing but the continuity equation of a compressible fluid of density ρ , and the classical mechanics Hamilton-Jacobi equation, respectively. The only unusual term regarding classical mechanics would be the potential energy term $Q(\vec{x}, t)$, which is called the Quantum Potential. It is equal to the curvature (Laplacian) and the steepness (magnitude of the gradient) of the density, normalized by the local magnitude of the density. That is, it is higher where the density gets locally “agglomerated” relative to its surrounding and is minimal when the density gets locally flat.

This decomposition is very well known and forms the basis of the Bohmian quantum theory [1, 2, 3] and Madelung's quantum hydrodynamics [4, 5].

Let us consider the Lagrangian frame of this configuration-space fluid. The velocity field guides the ensemble of Lagrangian trajectories $\vec{x}(\vec{\xi}, t)$ (which are called Bohmian trajectories), as

$$\frac{\partial \vec{x}(\vec{\xi}, t)}{\partial t} = \vec{v}(\vec{x}, t) \Big|_{\vec{x}=\vec{x}(\vec{\xi}, t)}, \quad (6)$$

such that each trajectory is tagged by $\vec{\xi}$, representing its positions at some reference time t_0 , $\vec{x}(\vec{\xi}, t_0) = \vec{\xi}$. Because of the existence and uniqueness theorems for the initial value problem, assuming $\vec{v}(\vec{x}, t)$ is regular, trajectories cannot cross each other in configuration space, meaning that the resulting label $\vec{\xi}$ for each trajectory is well-defined at all times.

In computational terms, these, so-called Bohmian trajectories, are privileged in front of other moving grids, due to the equivariance property [6] of the continuity equation, such that a countable, but big enough ensemble of them (bigger for an arbitrarily higher precision), will allow the reconstruction of the density ρ at all times t , by sampling them according to the density at some reference time t_0 . That is, one can understand the density ρ as the continuum limit density of such trajectories.

Formally, they are privileged since in their frame, equation (3) is equivalent to Newton's second law, linking the acceleration of the trajectory to the gradient of the total potential energy, also called total force. That is, for $k \in \{1, \dots, n\}$,

$$m_k \frac{\partial^2 x_k(\vec{\xi}, t)}{\partial t^2} = - \frac{\partial}{\partial x_k} \left[V(\vec{x}, t) + Q(\vec{x}, t) \right] \Big|_{\vec{x}=\vec{x}(\vec{\xi}, t)}. \quad (7)$$

With all, note that the density $\rho(\vec{x}, t)$ and the velocity field $\vec{v}(\vec{x}, t)$, both reconstructible from a big enough ensemble of Bohmian trajectories, contain exactly the same information as the wavefunction $\psi(\vec{x}, t)$, up to an irrelevant global phase. Thus, the time evolution of the quantum system can equivalently be described instead of using the Schrödinger Equation (1), by using Newton's second law (7) and the continuity equation (2). This shows the fundamental difference of quantum with classical mechanics. By (7), the curvature of the density (the agglomeration of all the trajectories) guides each individual trajectory, while by (2), the density itself is guided following the velocities of the individual trajectories. Thus, unlike in the classical Newton's law, it is not possible to exactly evolve a single trajectory, because the derivatives of the density require the knowledge of ρ over all trajectories around the one of interest. This also shows the quantum many-body problem. Increasing degrees of freedom imply exponentially more trajectories need to be simultaneously evolved.

If one reads literally this trajectory decomposition, the time evolution of an isolated quantum system (say, a quantum Universe), can be understood as an **uncountable** set of classical systems (a fluid of classical Universes), that repel each other when they get “tangentially close” to each other in configuration space (their density gets “agglomerated”). Let us call it the “Uncountable Tangent Universe” formulation. The natural question following this would be: what if in reality there are not an **uncountable** number of **tangent Universes**, but a (finite or infinite, but) **countable** number of them? Such that in the continuum limit, their interaction leads us to the quantum potential (5). This was first suggested by Hall et al. in [7], who baptised the new theory as the *Many Interacting World* theory (MIW). Here we will call it for clarity, the “Countable Tangent Universe” formulation.

¹By omission, “system”, we will refer to the whole Universe.

²If we considered a *closed* quantum system instead of an *isolated* one, the potential could be made to be time dependent.

1.1 A Swarm of Classical Universes

In this alternative to the quantum theory, for the description of a system, we would need to consider a countable set σ of trajectories, which assuming the non-crossing property for them, could still be indexed by $\vec{\xi}$, indicating their initial position as $\vec{x}^\xi(t_0) = \vec{\xi}$, with $\vec{\xi} \in \sigma$. Regarding their interactions, on the one hand, there would be the classical potential energy $V(\vec{x})$, ruling the interactions inside each Universe. We split it into two terms: $V_S(\vec{x}^\xi)$, due to the scenario's constraints (say, a wall, or a slit)³ and $V_{IP}(|x_k^\xi - x_j^\xi|)$, due to the inter-particle interactions within each Universe (the Coulomb potential, gravity etc.). On the other hand, as the only difference mathematically with respect to classical Newtonian mechanics, there would be an inter-Universe interaction as a function of the configuration of all the Universes, $W(\{\vec{x}^\eta\}_{\vec{\eta} \in \sigma})$. Finally, the dynamics of each trajectory would be guided by a generalized Newton's second law,

$$m_k \frac{d^2 x_k^\xi(t)}{dt^2} = -\frac{\partial}{\partial x_k} V(\vec{x}) \Big|_{\vec{x}=\vec{x}^\xi(t)} - \frac{\partial}{\partial x_k^\xi} W(\{\vec{x}^\eta\}_{\vec{\eta} \in \sigma}) \Big|_{\vec{x}^\eta=\vec{x}^\eta(t)} \quad (8)$$

with $k \in \{1, \dots, n\}$ and $\vec{\xi} \in \sigma$. Or more in general, in case any of the involved forces was non-conservative, beyond the Schrödinger equation, which only considers potential-gradient forces, we could have

$$m_k \frac{d^2 x_k^\xi(t)}{dt^2} = F_k(\vec{x}) \Big|_{\vec{x}=\vec{x}^\xi(t)} + G_k^\xi \left(\{\vec{x}^\eta\}_{\vec{\eta} \in \sigma} \right) \Big|_{\{\vec{x}^\eta(t)\}_{\vec{\eta} \in \sigma}}, \quad (9)$$

with $F_k(\vec{x})$, the total classical force on the k -th degree of freedom for a Universe with configuration \vec{x} , and with $G_k^\xi(\{\vec{x}^\eta\}_{\vec{\eta} \in \sigma})$ the total inter-Universe force on the k -th degree of freedom of the ξ -th Universe, for an ensemble of Universes at $\{\vec{x}^\eta\}_{\vec{\eta} \in \sigma}$.

Note that any such alternative theory should be demanded the recovery of the quantum Newton's second law (7) in the continuum limit (when σ gets to be uncountable).

2 OUR PROPOSAL

To our knowledge, the so-far published approaches to look for reasonable inter-Universe forces [7, 8, 9], have been limited to forces that rather take into account only the first neighbours in configuration-space, or are direct Lagrangian-frame approximations of (5). The first is certainly a computationally more affordable approach than interactions that directly imply arbitrarily far-away neighbours. Moreover, it has a direct analogy with the typical continuum limits taken in classical field theories, where the wave equation for example, is derived as the continuum limit of a countable set of harmonic oscillators connected to their nearest neighbours alone. However, non-locality is an intrinsic feature of quantum dynamics, the blame of which is actually (5), the potential we wish to approximate [1, 2, 3]. Moreover, both approaches still remain close to the Lagrangian frame methods to solve the SE [5, 10]. We here suggest a radically different force.

An interaction between trajectories that instantaneously only acts on the nearest neighbours is very atypical when considering the fundamental interactions of classical mechanics. Instead, either the Coulomb force, the Lorentz force or the gravitational force, among others, imply pair-wise forces between any two particles, no matter how far they are. Moreover, all these fundamental forces share a same analytical shape. The inverse distance of

any two particles, raised to a certain power (related arguably to the dimensionality of physical space and the propagation of "influence spheres"). This inverse distance is then multiplied by a fixed constant that gives the different forces a relative weight. A strict analogy appears to be the natural starting-point of the search for a force not limited to nearest neighbours, that describes a fundamental force (this time in configuration-space). For the $\vec{\xi}$ -th and the $\vec{\eta}$ -th universe, we suggest the interaction potential

$$W_{\xi,\eta}(\vec{x}^\xi, \vec{x}^\eta) = \frac{C}{||\vec{x}^\xi - \vec{x}^\eta||^B}, \quad (10)$$

with $|| \cdot ||$ the Euclidean norm and $C, B > 0$.⁴ The resulting configuration-space force on ξ by the η -th Universe would be

$$\vec{G}_{\xi,\eta} = \frac{A}{||\vec{x}^\xi - \vec{x}^\eta||^K} \hat{u}; \text{ where } \hat{u} := \frac{(\vec{x}^\xi - \vec{x}^\eta)}{||\vec{x}^\xi - \vec{x}^\eta||}, \quad (11)$$

and $A := C/B$, $K := B + 1$. With all, the total inter-Universe potential would read

$$W(\{\vec{x}^\eta\}_{\vec{\eta} \in \sigma}) = \frac{1}{2} \sum_{\vec{\xi}, \vec{\eta} \in \sigma} W_{\xi,\eta}(\vec{x}^\xi, \vec{x}^\eta). \quad (12)$$

It is important to note that C and B could depend on the dimensionality n of each Universe. This could happen in analogy with the Newtonian inverse power laws, which depend on the dimensionality of the considered space throughout which the influence of the particles is propagated. On the other hand, C and B could also depend on the number of trajectories considered, because the ideal continuum limit (5) is normalized by the density of Universes in each locality.

With all, we suggest the following steps in order to check if the proposed inter-Universe potential is plausible.

1. With an exploratory attitude, simulate the MIW approach in many different classical potentials $V(\vec{x})$, using inter-Universe forces $\vec{G}_{\xi,\eta}$ with different constants A, K and trying different dimensionalities of configuration-space n . Check if the characteristic signatures of quantum mechanics, absent in classical Newtonian mechanics, qualitatively emerge.
2. Analytically check the required conditions for the suggested inter-Universe interaction to be able to reproduce standard features related to the quantum potential, such as the properties of the total energy expectation.
3. With an exploitative attitude, employing many Universes (to emulate the continuum limit), optimize through simulations the parameters A, K that give the best fit to the predictions of the SE. Complete the optimization for several potentials $V(\vec{x})$ conveying different signatures of quantum mechanics, considering also different dimensionalities n . Check if there is any clear trend or correlation in the resulting fits (e.g. an induction rule for the optimals as a function of n).
4. If a trend is found using enough trajectories, analytically check if the induced inter-Universe force allows the correct continuum limit.

In the present manuscript, we give the implementation of a general framework to elucidate points 1 and 3 in an automatized way, together with the results of point 1.

³If the system is the whole Universe, this term would be zero, for it reflects the interaction with external particles.

⁴We consider that they exert a repulsive force to each other.

3 METHODS

3.1 Solving the Uncountable Tangent Universes

In order to solve the general SE, let us generalize the Crank-Nicolson method given by [11] for $n = 1$ to an arbitrary n .

First note that knowing the state of the wavefunction at a certain time $\psi(\vec{x}, t)$, the SE (1) can formally be solved as

$$\psi(\vec{x}, t + k\Delta t) = \hat{U}_{\vec{x}, \Delta t}^k \psi(\vec{x}, t), \text{ for } k \in \mathbb{N}; \Delta t \in \mathbb{R}, \quad (13)$$

by considering the Hamiltonian $\hat{H}_{\vec{x}} := -\frac{\hbar^2}{2m_k} \sum_{k=1}^N \frac{\partial^2}{\partial x_k^2} + V(\vec{x})$ and the unitary⁵ operator $\hat{U}_{\vec{x}, \Delta t} := e^{-\frac{i}{\hbar} \Delta t \hat{H}_{\vec{x}}}$. The exponential of an operator \hat{A} is defined as $e^{\hat{A}} := \sum_{k=0}^{\infty} \hat{A}^k / k!$, which for $\hat{U}_{\vec{x}, \Delta t}$ and a small enough Δt , implies terms that are each time smaller. A trivial approximation of $\hat{U}_{\vec{x}, \Delta t}$ by truncation however, is not unitary. We can get an approximated propagator that is unitary, after noticing that by the unitarity of $\hat{U}_{\vec{x}, \Delta t}$ and the Hermiticity of $\hat{H}_{\vec{x}}$, $\hat{U}_{\vec{x}, \Delta t}^{-1} = \hat{U}_{\vec{x}, \Delta t}^\dagger = \hat{U}_{\vec{x}, -\Delta t}$. This implies that $\hat{U}_{\vec{x}, \Delta t} = \hat{U}_{\frac{\Delta t}{2}} \hat{U}_{\frac{\Delta t}{2}} = \hat{U}_{-\frac{\Delta t}{2}}^{-1} \hat{U}_{\frac{\Delta t}{2}}$, such that the truncation of the factors at order N ,

$$\hat{U}_{\vec{x}, \Delta t} \simeq \left(\sum_{k=0}^N \frac{1}{k!} \left[\frac{i}{\hbar} \hat{H}_{\vec{x}} \frac{\Delta t}{2} \right]^k \right)^{-1} \sum_{k=0}^N \frac{1}{k!} \left[\frac{-i}{\hbar} \hat{H}_{\vec{x}} \frac{\Delta t}{2} \right]^k \quad (14)$$

is now trivially unitary. Moreover, inserting such a truncated $\hat{U}_{\vec{x}, \Delta t}$ in (13), one gets a correct approximation of the Schrödinger Equation till order N in Δt , as can be seen by direct inspection. In our implementation, following [11], we only leave the terms to first order, such that $\hat{U}_{\vec{x}, \Delta t} \simeq (\hat{I}d + \frac{i}{\hbar} \hat{H}_{\vec{x}} \frac{\Delta t}{2})^{-1} (\hat{I}d - \frac{i}{\hbar} \hat{H}_{\vec{x}} \frac{\Delta t}{2})$. This leaves the approximated SE,

$$\left(\hat{I}d + \frac{i}{\hbar} \hat{H}_{\vec{x}} \frac{\Delta t}{2} \right) \psi(\vec{x}, t + \Delta t) = \left(\hat{I}d - \frac{i}{\hbar} \hat{H}_{\vec{x}} \frac{\Delta t}{2} \right) \psi(\vec{x}, t). \quad (15)$$

Finally, by defining a discrete grid in space and using a finite difference approximation of the second derivative, we end up converting the SE (1) into an iterative linear equation resolution problem. Further details of the generalized scheme we suggest, are given in Appendix B. Note that we considered a rectangular simulation domain Ω , with reflecting boundary conditions, meaning $\psi(\vec{x}, t) = 0 \forall \vec{x} \in \partial\Omega$.

For the computation of the Bohmian trajectories, as it is typically done, we computed the velocity field (4), with the computationally more suitable form,

$$v_k(\vec{x}, t) = \frac{\hbar}{m_k} \operatorname{Im} \left\{ \frac{1}{\psi(\vec{x}, t)} \frac{\partial \psi(\vec{x}, t)}{\partial x_k} \right\}. \quad (16)$$

Considering a grid step Δx_k for the x_k axis, the gradient of the wavefunction was calculated with the fourth order centered difference,

$$\begin{aligned} \frac{\partial \psi(\vec{x}, t)}{\partial x_k} &= \frac{1}{12\Delta x_k} \left(-\psi(\vec{x} + 2\Delta x_k, t) + 8\psi(\vec{x} + \Delta x, t) \right. \\ &\quad \left. - 8\psi(\vec{x} - \Delta x, t) + \psi(\vec{x} - 2\Delta x, t) \right) + O(\Delta x_k^4). \end{aligned} \quad (17)$$

Given the initial wavefunction $\psi(\vec{x}, t_0)$, we randomly sample a set σ of M initial trajectory positions $\{\vec{\xi}\}_{\xi \in \sigma}$. We detail in Appendix D, a very important problem we faced in the sampling.

⁵An operator \hat{A} is unitary if $\hat{A}^\dagger \hat{A} = \hat{I}d$, with \cdot^\dagger the Hermitian conjugate. If there is an inverse of \hat{A} , by its uniqueness, $\hat{A}^{-1} = \hat{A}^\dagger$, with \cdot^{-1} the inverse.

Once we have the initial positions $\{\vec{\xi}\}_{\xi \in \sigma}$, we evolve them using the velocity field (16) over the discretized spatial grid. We compute the linear interpolation of the velocity field on the trajectories, the set $\{\vec{v}^\xi(t)\}_{\xi \in \sigma}$, which using a simple Euler rule gives $\vec{x}^\xi(t + \Delta t) \simeq \vec{x}^\xi(t) + \vec{v}^\xi(t) \Delta t$.

3.2 Solving the Countable Tangent Universes

In order to solve Newton's second law with the inter-Universe interaction (8), we use the Verlet algorithm [12], which allows the conservation of total energy in time.

Essentially, it consists on expanding the trajectory $\vec{x}^\xi(t + \varepsilon)$ in Taylor series for both $\varepsilon \in \{\Delta t, -\Delta t\}$, such that after adding them we get,

$$\vec{x}^\xi(t + \Delta t) + \vec{x}^\xi(t - \Delta t) = 2\vec{x}^\xi(t) + \frac{d^2 \vec{x}^\xi(t)}{dt^2} \Delta t^2 + O(\Delta t^4). \quad (18)$$

This allows the determination of the trajectory at a new time $t + \Delta t$, to fourth order, by only knowing where it was at t and $t - \Delta t$, plus knowing its acceleration at t , which can be directly known through Newton's second law (8). With it, if needed, the velocity of the Universes can also be directly computed, with a simple Euler rule, as $\vec{v}^\xi(t + \Delta t) \simeq \vec{v}^\xi(t) + \frac{d^2 \vec{x}^\xi(t)}{dt^2} \Delta t$.

In the interest of comparison with the Eulerian frame SE (1), on the one hand, we considered a finite domain Ω , with elastic reflecting boundary conditions. On the other hand, we estimated an Eulerian frame density $\rho(\vec{x}, t)$ and velocity field $\vec{v}(\vec{x}, t)$ from the trajectories. For the density field we employed a Gaussian kernel centered in each of the trajectories,

$$\rho(\vec{x}, t) \simeq \mathcal{N} \sum_{\vec{\xi} \in \sigma} \exp \left(-\frac{\|\vec{x} - \vec{x}^\xi(t)\|^2}{2s^2} \right) \quad (19)$$

with \mathcal{N} a normalization factor such that $\int_{\Omega} \rho(\vec{x}, t) dx = 1$, and $s > 0$ a hyper-parameter that we fix to $s = 1$. Note that there are good algorithms to estimate the best bandwidth s , as explained by [13], but we leave this as future work. Finally, the velocity field was estimated by a k nearest neighbors approach, such that the velocity at the Eulerian configuration \vec{x} is estimated as the average velocity of the k nearest trajectories to \vec{x} at that time t . We define the set of their labels as $\sigma_{\vec{x}}$. In particular, the average is weighted by the relative distance of the neighbor, such that,

$$\vec{v}(\vec{x}, t) \simeq \frac{\sum_{\vec{\xi} \in \sigma_{\vec{x}}} \frac{1}{\|\vec{x} - \vec{x}^\xi(t)\|} \vec{v}^\xi(t)}{\sum_{\vec{\xi} \in \sigma_{\vec{x}}} \frac{1}{\|\vec{x} - \vec{x}^\xi(t)\|}}. \quad (20)$$

It is worth noting that while in the Eulerian frame SE (1), the trajectories are *a-posteriori*, in the sense that they are optionally computed from the density and velocity field once we know them, in the MIW approach it is just the opposite: it is the density and velocity fields that are *a-posteriori* obtained from the trajectories and their velocities.

4 THE IMPLEMENTATION

In order to tackle the proposal, we implemented an open source Python framework that can be found in our Github repository [14]. Among others, the framework includes some “sandbox” Jupyter Notebooks to try custom initial conditions, potential energies and inter-Universe forces, for the SE with $n \in \{1, 2, 3\}$ or the MIW approach with an arbitrary n . It also contains scripts to

plot the results, the employed source files for the parallelization of a search grid for the optimal force of the suggested shape (11) and scripts for its posterior data analysis.

The core numerical calculations were made with the `numpy` [15] and `scipy` [16] libraries, while plotting was done with `matplotlib` [17]. An optional GPU calculation mode was also implemented with the `cupy` library [18] (requiring CUDA), which adapts the `numpy` and `scipy` codes conveniently.

The coefficient matrices of the SE solver of section 3.1 are sparse (as explained in Appendix B), so we employed sparse matrix memory management and algebra, as provided by `scipy` and `cupy`. In particular, a suitable LU decomposition algorithm was chosen for their resolution.

Finally, employing the `multiprocessing` standard library, coordinator scripts were written to calculate in parallel CPU processes, different potential energy scenarios with different conditions and variant parameters for the ansatz inter-Universe force.

For more details on the implementation, check the repository [14].

5 RESULTS OF THE EXPLORATORY SEARCH

In Appendix A, we show some results cherry-picked from the exploratory search. As we proceed to explain now, they show that the suggested inter-Universe force (11) is capable of capturing intrinsically quantum features that are completely absent in classical mechanics (CM)⁶.

Most of the signatures of quantum mechanics can already be featured qualitatively in $n = 1$, including the broadening of wave-packets, stationary states, quantum tunneling and self-interference patterns. The only quantum signature necessarily demanding a higher dimensionality is the quantum entanglement, inherent to $n > 1$. Consequently, in what follows, we show $n = 1$ and $n = 2$ cases featuring these signatures, and just show a pair of $n = 3$ results, for the sake of completeness.⁷

In Figure 1, left column, we consider a free $n = 1$ particle, that shows the characteristic broadening of the wavepackets due to the quantum potential (see a SE simulation in (a) and (b)). In panel (c) we show that our MIW approach correctly captures this behavior, while in panel (d), we see that classical particles would remain stationary at all times. We confirm these results for $n = 2$ and $n = 3$ particles in Figures 4 and 6.

In the right column of Figure 1, we simulate a harmonic potential quantum system, for the well-known Gaussian ground state, possessing the quantum mechanical property of stationarity (see panels (e) and (f)). While in the analogous classical system, in panel (h), the trajectories collapse into the minimum of the potential, we can see in panel (g), that the inter-Universe force sustains the trajectories around their initial positions, reproducing the quantum stationarity. Note as indicated in the figure by the arrows, that with the chosen parameters for the inter-Universe force, the Gaussian state still is not really an exact stationary state in our MIW. It slightly vibrates in a “breathing” manner. We leave as future work the quantitative optimization of the force parameters that lead to even more stable proofs of stationarity.

⁶We refer to CM as the particular case of MIW with a zero inter-Universe force, implying independent Universe trajectories that do not “bounce” with each other in configuration-space and have the possibility to cross each other. They just represent the classical time evolution of different initial conditions.

⁷Of course, for a quantitative exploration of the optimal force, an equally exhaustive analysis of the $n = 3$ case would be required.

For now, in Figures 4 and 6, in the right columns, we also show the quasi-stationarity for $n = 2$ and $n = 3$, using the harmonic and hydrogen atom potentials respectively.

In Figure 2, left column, we simulate a wavepacket impinging against a potential energy barrier. As it can be seen in the classical mechanics panel, (d), the energy of the barrier is too high compared to the kinetic energy of the trajectories and they would classically be expected to bounce back. However, both in the SE evolution and in our MIW approach, there is part of the trajectories that do cross the barrier (due to the pressure of the other trajectories). This is called quantum tunneling. Moreover, note that when the main core of the density is reflected, it interferes with the outermost edge of the wavefunction, generating an interference pattern of three peaks. This as well is clearly captured by our MIW approach.

In Figure 3, we simulate a more explicit case of self-interference, where the two modes of an initially split wavepacket are thrown against each other. While we see in panel (h) that the CM trajectories do not generate any interference pattern, we see in (f) and (g) that the SE and MIW densities clearly generate a three-mode interference pattern. Due to its capital importance in the prediction of quantum phenomena, we confirm self-interference is safely captured by our MIW method also in $n = 2$ and $n = 3$, in Figures 4 and ??.

Finally, we show in Figure 4, right column, that our MIW approach is capable of reproducing quantum entanglement as well. For this, we consider a bottleneck potential that form a free entrance into a tunnel. As proved by [19], the confinement in the y axis inside the tunnel causes a “virtual” barrier for the transport along x . In particular, if the energy of the wavepacket kicked in x is smaller than the eigenenergy of the transversal section eigenstates in y , the wavepacket is mostly reflected by the entrance to the tunnel. Just as if there was a potential energy barrier in that entrance (where nonetheless, $V(x, y) = 0$). This effect is purely due to the non-factorizability of the Hamiltonian. Interestingly, on top of that, due to the quantum tunneling effect, a small part of the density will still cross the entanglement-induced barrier. As we can see in Figure 5, unlike the CM trajectories, that seemingly cross the tunnel, without acknowledging any entanglement-induced barrier, both the SE and our MIW approach, successfully reflect most of the wavepacket, as demanded by the xy coupling.

5.1 Towards Quantitativeness

In order to perform the exploratory search, we simulated a grid of 8×8 values of K and A for about 7 scenarios per dimension $n \in \{1, 2, 3\}$ (all of which can be found in the implemented framework [14]). After computing quantitative metrics to compare them to reference SE simulations (metrics we describe in Appendix D), we found that the best values of K, A for different scenarios were very similar between each other, within the same n , while they changed significantly for increasing n . In particular, as we gather for the trajectory divergence metric in Figure 1, we found signs indicating the optimal K, A for $n = 1$ may lay around $K = 0.6, 0.2$ and $A = 1.0, 0.1$. For $n = 2$, the optimal appears to be closer to $K = 1.0, A = 1.0$, while for $n = 3$, $K = 4.0, 2.0, A = 1.0, 3.0$ appear to be better candidates. With all, for an increasing dimensionality of the configuration space, the inter-Universe force that best approaches the quantum potential’s predictions appears to have an increasing power K .

6 CONCLUSIONS

In a nutshell, we have confirmed that a configuration-space force for countable classical Universes, with a shape akin to the classical fundamental forces (which are inverse distance power laws), qualitatively reproduces the characteristic signatures of quantum mechanics, including entanglement and self-interference, among others. Moreover, we have found signs that indicate that such a force does not depend on the classical forces acting besides it, even if the power law of the force appears to depend on the dimensionality of configuration-space (just as happens with classical forces regarding physical space dimensionality).

To do this we have implemented an open source framework that allows the continuation of the study, now with a quantitative optimization of the suggested force as objective. This is left as future work, together with the analytical study of the suggested force, as explained in the project proposal in section 2.

REFERENCES

- [1] D. Bohm, “A suggested interpretation of the quantum theory in terms of “hidden” variables. i,” *Physical review*, vol. 85, no. 2, p. 166, 1952.
- [2] P. R. Holland, *The quantum theory of motion: an account of the de Broglie-Bohm causal interpretation of quantum mechanics*. Cambridge university press, 1995.
- [3] X. O. Pladenvall and J. Mompart, *Applied Bohmian mechanics: From nanoscale systems to cosmology*. CRC Press, 2019.
- [4] E. Madelung, “Quantum theory in hydrodynamical form,” *Z. Phys*, vol. 40, p. 322, 1927.
- [5] R. E. Wyatt, *Quantum dynamics with trajectories: introduction to quantum hydrodynamics*, vol. 28. Springer Science & Business Media, 2005.
- [6] D. Dürr, S. Goldstein, and N. Zanghi, “Quantum equilibrium and the origin of absolute uncertainty,” *Journal of Statistical Physics*, vol. 67, pp. 843–907, 1992.
- [7] M. J. Hall, D.-A. Deckert, and H. M. Wiseman, “Quantum phenomena modeled by interactions between many classical worlds,” *Physical Review X*, vol. 4, no. 4, p. 041013, 2014.
- [8] H. Herrmann, M. J. Hall, H. M. Wiseman, and D.-A. Deckert, “Ground states in the many interacting worlds approach,” *arXiv preprint arXiv:1712.01918*, 2017.
- [9] S. Sturniolo, “Computational applications of the many-interacting-worlds interpretation of quantum mechanics,” *Physical Review E*, vol. 97, no. 5, p. 053311, 2018.
- [10] X. Oianguren-Asua, “Quantum dynamics with waves and trajectories.” https://github.com/Oiangu9/Bohmian_Research_Lab_QuantumCAT/blob/main/Quantum_Dynamics_with_Waves_and_Trajectories.pdf.
- [11] W. H. Press, S. A. Teukolsky, W. T. Vetterling, and B. P. Flannery, *Numerical recipes 3rd edition: The art of scientific computing*. Cambridge university press, 2007.
- [12] D. Frenkel, B. Smit, and M. A. Ratner, *Understanding molecular simulation: from algorithms to applications*, vol. 2. Academic press San Diego, 1996.
- [13] S. J. Sheather, “Density estimation,” *Statistical science*, pp. 588–597, 2004.
- [14] “Github repository with the python scripts and notebook generated for the project.” https://github.com/Oiangu9/Countable_vs_Uncountable_Tangent_Universes.
- [15] C. R. H. et al, “Array programming with NumPy,” *Nature*, vol. 585, pp. 357–362, Sept. 2020.
- [16] P. e. a. Virtanen, “SciPy 1.0: Fundamental Algorithms for Scientific Computing in Python,” *Nature Methods*, vol. 17, pp. 261–272, 2020.
- [17] J. D. Hunter, “Matplotlib: A 2d graphics environment,” *Computing in Science & Engineering*, vol. 9, no. 3, pp. 90–95, 2007.
- [18] R. Okuta, Y. Unno, D. Nishino, S. Hido, and C. Loomis, “Cupy: A numpy-compatible library for nvidia gpu calculations,” in *Proceedings of Workshop on Machine Learning Systems (LearningSys) in The Thirty-first Annual Conference on Neural Information Processing Systems (NIPS)*, 2017.
- [19] D. Pandey, X. Oriols, and G. Albareda, “Effective 1d time-dependent schrödinger equations for 3d geometrically correlated systems,” *Materials*, vol. 13, no. 13, p. 3033, 2020.
- [20] “Wikipedia entry on the rejection sampling algorithm.” https://en.wikipedia.org/wiki/Rejection_sampling.
- [21] X. Oianguren-Asua, C. F. Destefani, M. Villani, D. K. Ferry, and X. Oriols, “Bohmian mechanics as a practical tool,” *arXiv preprint arXiv:2212.09671*, 2022.

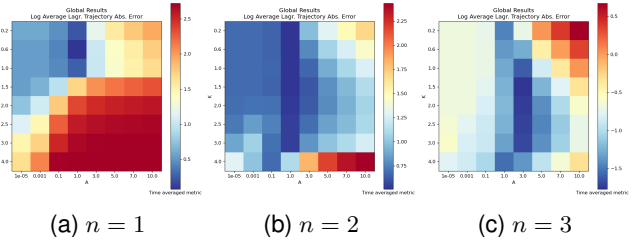


Figure 1: The colormaps show the logarithm of metric (35), defied to compare the SE simulations to our MIW simulations. It measures the divergence between the MIW and Bohmian trajectories. The plotted numbers are the averages per K, A over all the explored scenarios, which can be found in [14]. An average of 7 different potential energy profiles are included per n . Abscissa is A , ordinate is K . In atomic units.

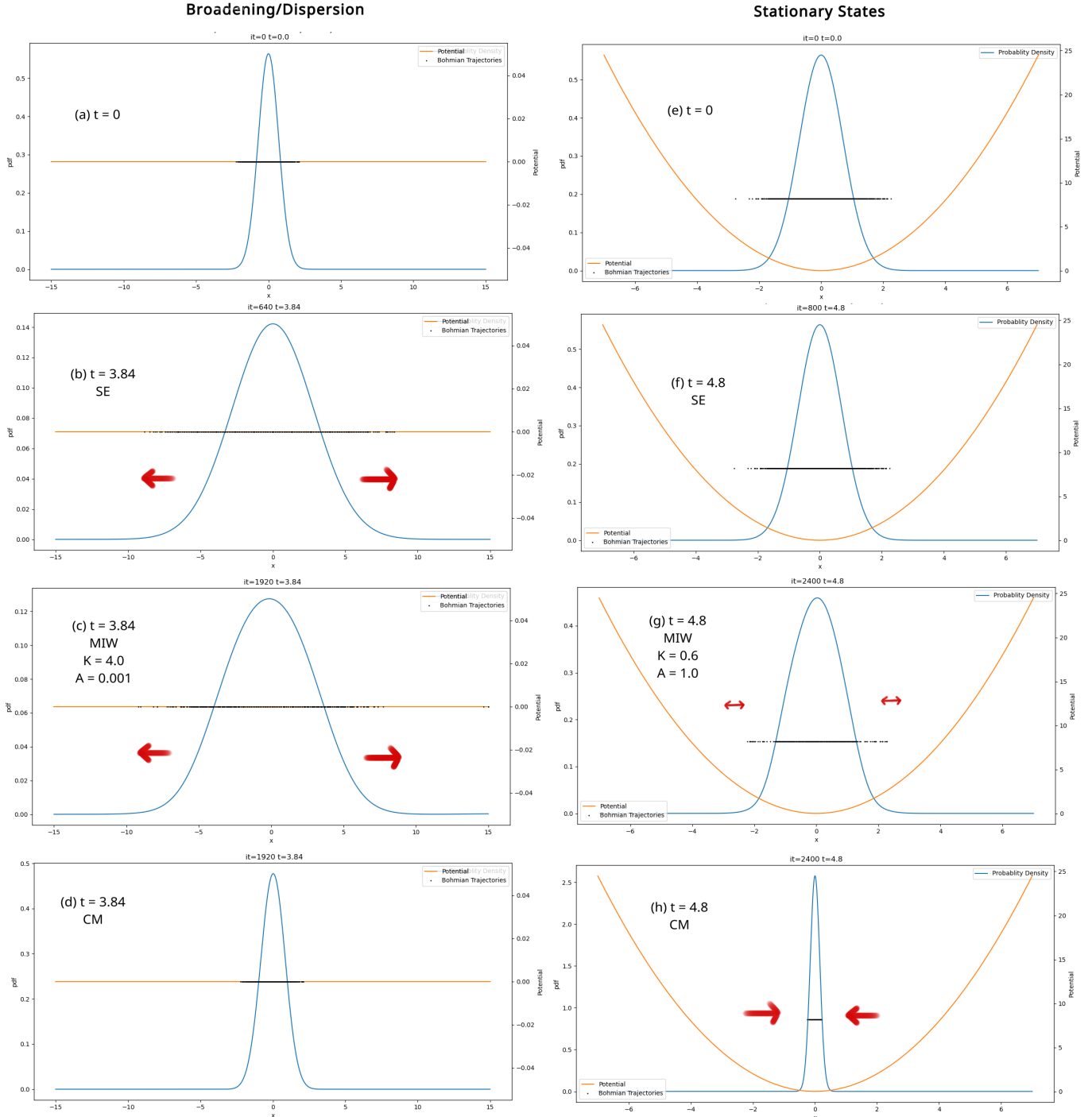
A: RESULT PLOTS


Figure 2: Results of the $n = 1$ exploratory search that show how the MIW approach with the suggested potential is capable of reproducing purely quantum effects like the broadening or dispersion of a wavepacket and stationary states. The first row shows the initial configuration of the system common to all, the SE, MIW and CM approach. In the second row, the SE result a time later is shown. In the third row, the MIW result and in the last row the CM result. In blue the probability density is represented, in black, the sampled trajectories (there are 3000 in all cases) and in orange, the potential energy profile. The red arrows indicate qualitatively the momenta of the ensemble of trajectories, for a qualitative understanding of the dynamics. All in atomic units.

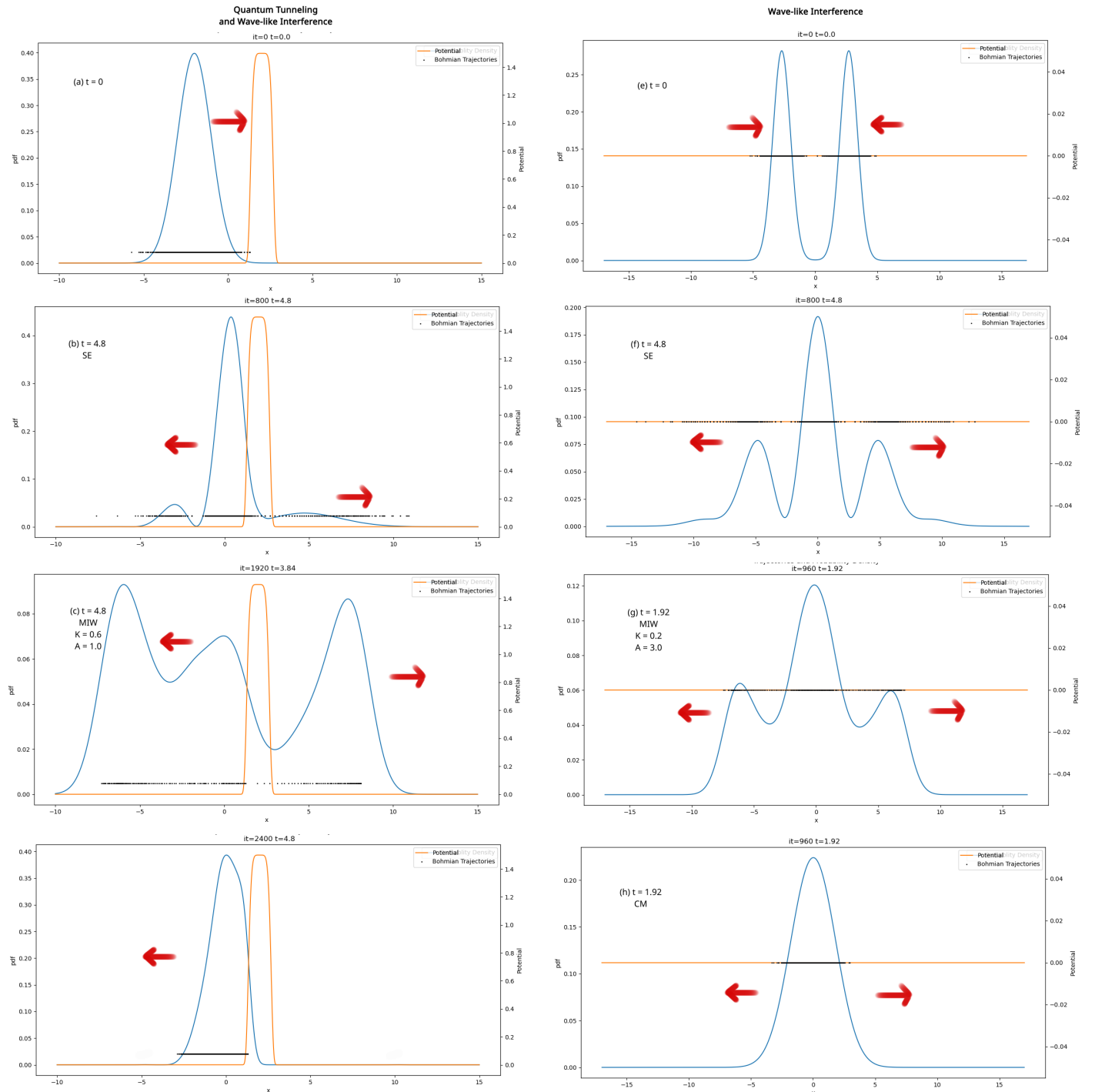


Figure 3: Results of the $n = 1$ exploratory search that show how the MIW approach with the suggested potential is capable of reproducing purely quantum effects like the quantum tunneling and wave-like interference patterns, as indicated by the headers of the columns. The first row shows the initial configuration of the system, common to all, the SE, MIW and CM approach. In the second row, the SE result a time later is shown. In the third row, the MIW result and in the last row the CM result. In blue the probability density is represented, in black, the sampled trajectories (there are 3000 in all cases) and in orange, the potential energy profile. The red arrows indicate qualitatively the momenta of the ensemble of trajectories, for a qualitative understanding of the dynamics. All in atomic units.

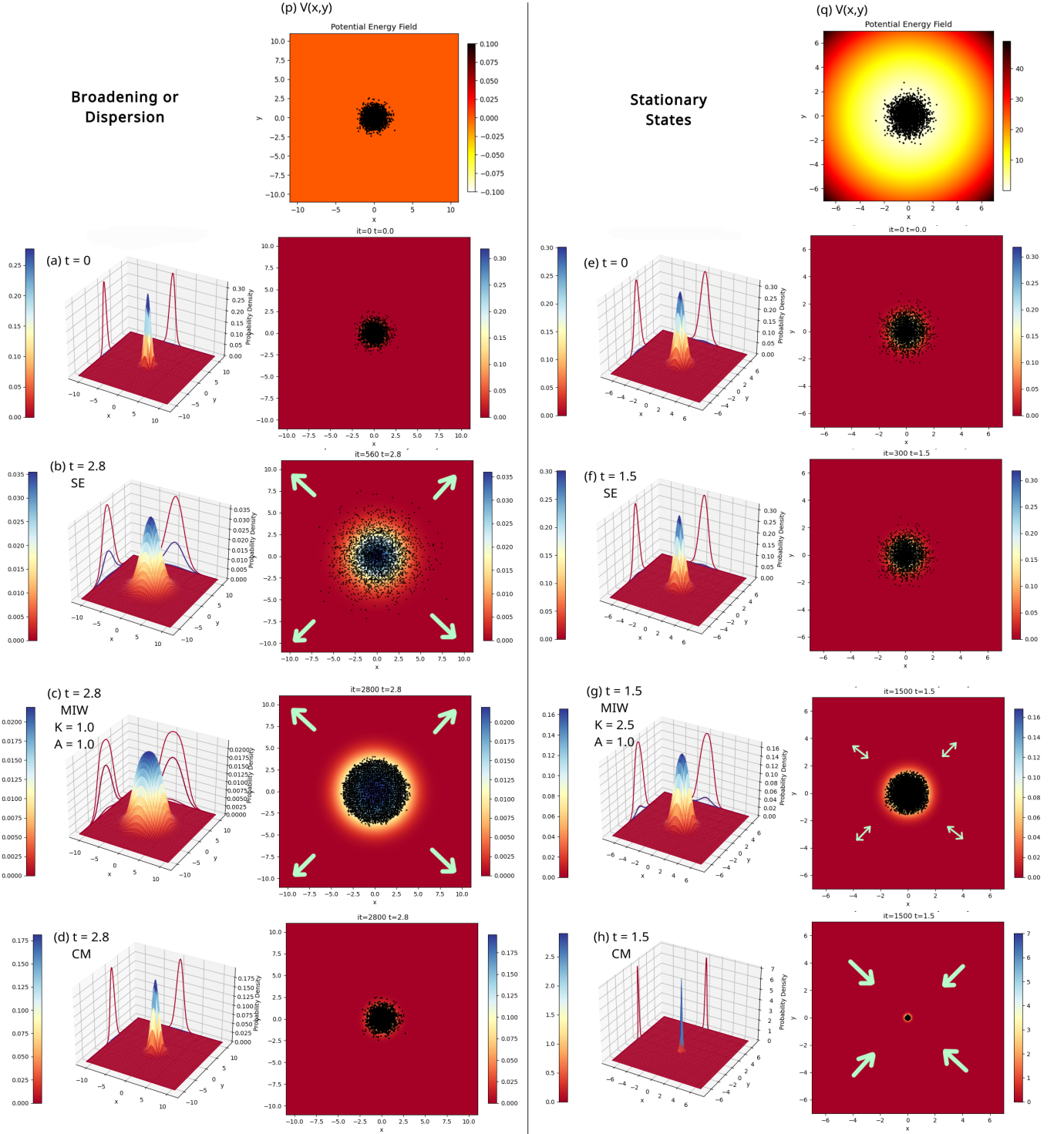


Figure 4: Results of the $n = 2$ exploratory search that show how the MIW approach with the suggested potential is capable of reproducing purely quantum effects like the broadening or dispersion of a wavepacket and stationary states. The first row shows the initial configuration of the system, common to all, the SE, MIW and CM approach. In the second row, the SE result a time later is shown. In the third row, the MIW result and in the last row the CM result. The heatmap represents the probability density, either in 3D or in 2D within each subplot. In 3D, some projected contour plots can be seen. In black, the sampled trajectories (there are 3000 in all cases), the potential energy profile. The green arrows indicate qualitatively the momenta of the ensemble of trajectories, for a qualitative understanding of the dynamics. All in atomic units.

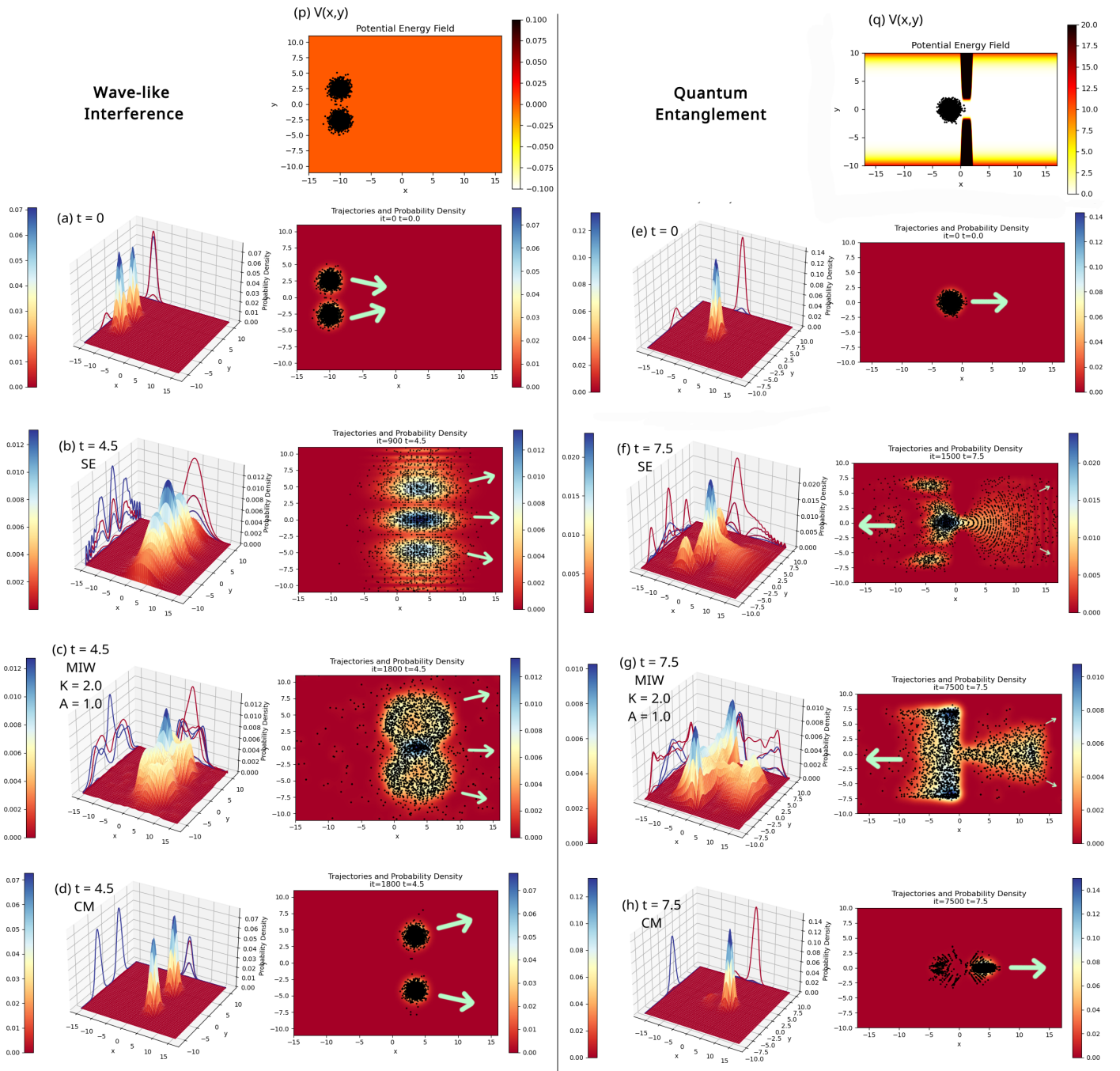


Figure 5: Results of the $n = 2$ exploratory search that show how the MIW approach with the suggested potential is capable of reproducing purely quantum effects, like quantum entanglement, tunneling and wave-like self-interference. The first row shows the initial configuration of the system, common to all, the SE, MIW and CM approach. In the second row, the SE result a time later is shown. In the third row, the MIW result and in the last row the CM result. The heatmap represents the probability density, either in 3D or in 2D within each subplot. In 3D, some projected contour plots can be seen. In black, the sampled trajectories (there are 3000 in all cases), the potential energy profile. The green arrows indicate qualitatively the momenta of the ensemble of trajectories, for a qualitative understanding of the dynamics. All in atomic units.

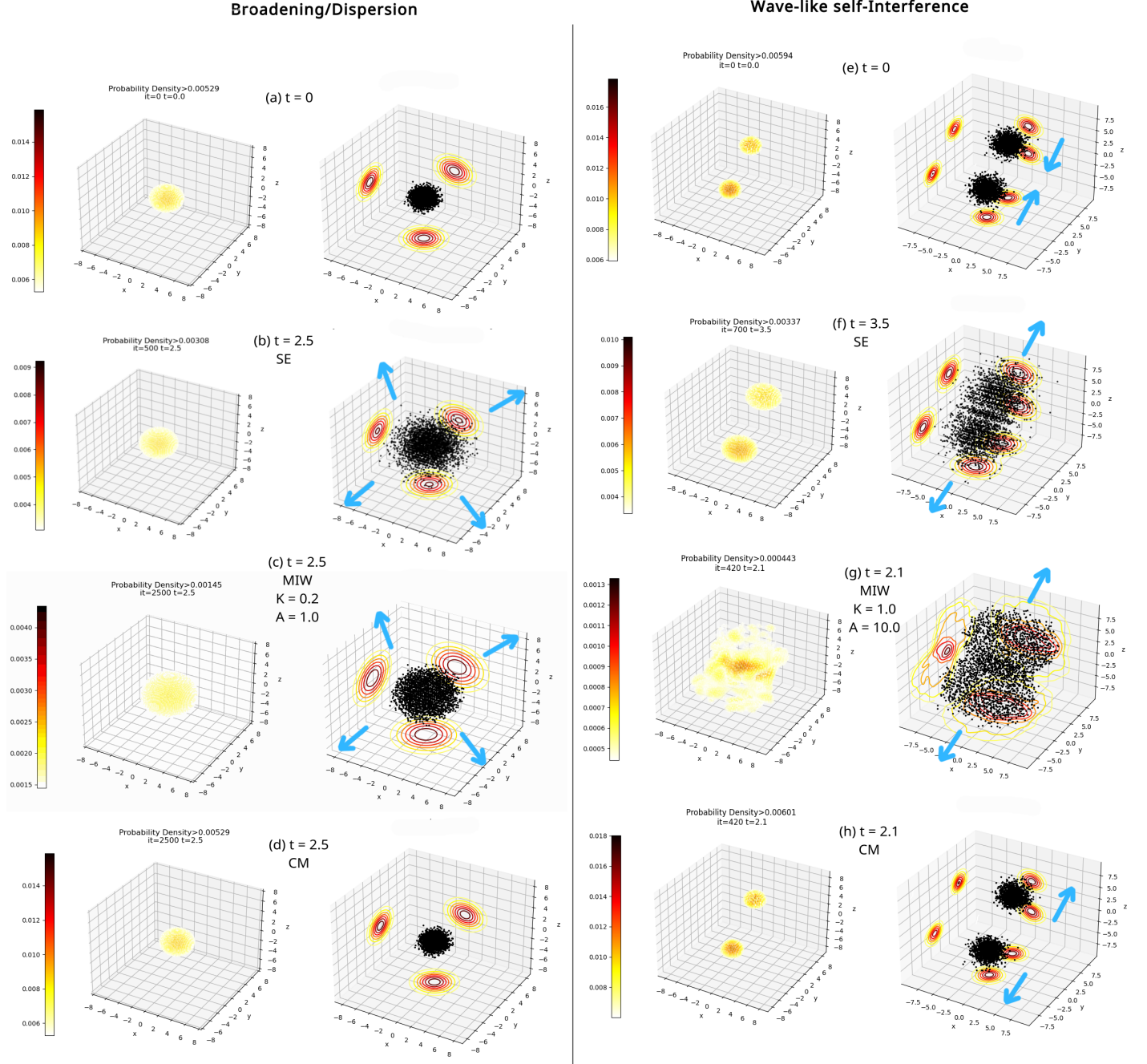


Figure 6: Results of the $n = 3$ exploratory search that show how the MIW approach with the suggested potential is capable of reproducing purely quantum effects like wave-like self-interferences or stationary states. The first row shows the initial configuration of the system, common to all, the SE, MIW and CM approach. In the second row, the SE result a time later is shown. In the third row, the MIW result and in the last row the CM result. In the left subplots, we see the set of points with a probability density greater than a third of the maximum at that time, while in the right subplots, we see in black, the sampled trajectories (there are 3000 in all cases), and the projected probability density contour plots in the coordinate planes. The green arrows indicate qualitatively the momenta of the ensemble of trajectories, for a qualitative understanding of the dynamics. All in atomic units.

B: A GENERALIZED CRACK-NICOLSON SCHRÖDINGER EQUATION SOLVER

Following the equations of Section 3.1, in this appendix, we present a generalized Crank-Nicolson scheme to solve the Schrödinger equation of n degrees of freedom.

First of all, let us introduce an equi-spaced discretization into the spatial degrees of freedom $\{x_1, \dots, x_n\}$, being $\{J_{x_1}, \dots, J_{x_n}\}$ the total number of intervals in which we discretize them. If we denote by $x_{k_{max}}$ and $x_{k_{min}}$ the two endpoints of the k -th axis and the grid step of that axis is $\Delta x_k := (x_{k_{max}} - x_{k_{min}})/J_{x_k}$, the considered spatial points in the grid will be $x_k^{(j)} := x_{k_{min}} + j\Delta x_k$, with $j \in \{0, 1, 2, \dots, J_{x_k}\}$ and $k \in \{1 \dots n\}$.

For notational convenience we will write the wave-function $\psi(\vec{x}, t)$ as a function of the indices of the nodes in the grid, specifying the time as a superindex. E.g.,

$$\psi_{(j_1, j_2, \dots, j_n)}^{(t)} := \psi(x_1^{(j_1)}, x_2^{(j_2)}, \dots, x_n^{(j_n)}, t), \quad (21)$$

For the spatial partial derivatives we will use the second order finite difference,

$$\frac{\partial^2}{\partial x_k^2} \psi_{(j_1, \dots, j_k, \dots, j_n)}^{(t)} = \frac{\psi_{(j_1, \dots, j_{k+1}, \dots, j_n)}^{(t)} - 2\psi_{(j_1, \dots, j_k, \dots, j_n)}^{(t)} + \psi_{(j_1, \dots, j_{k-1}, \dots, j_n)}^{(t)}}{(\Delta x_k)^2} + o((\Delta x_k)^2). \quad (22)$$

Then, introducing it all into equation (15), we get a discretized unitary approximation of the SE,

$$\begin{aligned} \psi_{(j_1, \dots, j_n)}^{(t+\Delta t)} - \frac{i\Delta t}{2\hbar} \left[\sum_{k=1}^n \frac{\hbar^2}{2m_k} \left(\frac{\psi_{(j_1, \dots, j_{k+1}, \dots, j_n)}^{(t+\Delta t)} - 2\psi_{(j_1, \dots, j_k, \dots, j_n)}^{(t+\Delta t)} + \psi_{(j_1, \dots, j_{k-1}, \dots, j_n)}^{(t+\Delta t)}}{(\Delta x_k)^2} \right) - V_{j_1, \dots, j_n} \psi_{(j_1, \dots, j_n)}^{(t+\Delta t)} \right] = \\ = \psi_{(j_1, \dots, j_n)}^{(t)} + \frac{i\Delta t}{2\hbar} \left[\sum_{k=1}^n \frac{\hbar^2}{2m_k} \left(\frac{\psi_{(j_1, \dots, j_{k+1}, \dots, j_n)}^{(t)} - 2\psi_{(j_1, \dots, j_k, \dots, j_n)}^{(t)} + \psi_{(j_1, \dots, j_{k-1}, \dots, j_n)}^{(t)}}{(\Delta x_k)^2} \right) - V_{j_1, \dots, j_n} \psi_{(j_1, \dots, j_n)}^{(t)} \right], \end{aligned} \quad (23)$$

which can be rewritten as the master equation of the Crank-Nicolson method,

$$\begin{aligned} b_{(j_1, \dots, j_n)} \psi_{(j_1, \dots, j_n)}^{(t+\Delta t)} + \sum_{k=1}^n a_k \left(\psi_{(j_1, \dots, j_{k-1}, \dots, j_n)}^{(t+\Delta t)} + \psi_{(j_1, \dots, j_{k+1}, \dots, j_n)}^{(t+\Delta t)} \right) = \\ = d_{(j_1, \dots, j_n)} \psi_{(j_1, \dots, j_n)}^{(t)} - \sum_{k=1}^n a_k \left(\psi_{(j_1, \dots, j_{k-1}, \dots, j_n)}^{(t)} + \psi_{(j_1, \dots, j_{k+1}, \dots, j_n)}^{(t)} \right), \end{aligned} \quad (24)$$

gathering together the next time independent coefficients,

$$b_{(j_1, \dots, j_n)} := 1 + \frac{i\Delta t \hbar}{2} \sum_{k=1}^n \left(\frac{1}{m_k (\Delta x_k)^2} \right) + \frac{i\Delta t}{2\hbar} V_{(j_1, \dots, j_n)}, \quad (25)$$

$$d_{(j_1, \dots, j_n)} := 1 - \frac{i\Delta t \hbar}{2} \sum_{k=1}^n \left(\frac{1}{m_k (\Delta x_k)^2} \right) - \frac{i\Delta t}{2\hbar} V_{(j_1, \dots, j_n)}, \quad (26)$$

$$a_k := -\frac{i\Delta t \hbar}{4m_k (\Delta x_k)^2}. \quad (27)$$

Note that $b_{(j_1, \dots, j_n)} = d_{(j_1, \dots, j_n)}^*$.

The master equation (24) is nothing but a linear equation system, where given the coefficients $b_{(j_1, \dots, j_n)}$, a_k and the wavefunction at time t , $\psi_{(j_1, \dots, j_n)}^{(t)}$, allows the determination of the wavefunction a time Δt later, $\psi_{(j_1, \dots, j_n)}^{(t+\Delta t)}$. In order to solve it using algebraic matrix equations, we flatten the tensorial wavefunction over the spatial grid, defining the vector,

$$\vec{\psi}^{(t)} := \left(\psi_{(0,0,0\dots 0)}^{(t)}, \dots, \psi_{(J_{q1},0,0\dots 0)}^{cur}, \psi_{(0,1,0\dots 0)}^{(t)}, \dots, \psi_{(J_{q1},1,0\dots 0)}^{(t)}, \dots, \psi_{(J_{q1},J_{q2},0\dots 0)}^{(t)}, \dots, \psi_{(J_{q1},\dots,J_{qn})}^{(t)} \right) \in \mathbb{C}^{(J_{q1}+1)\cdots(J_{qn}+1)} \quad (28)$$

With this, it is possible to rewrite (24) as a matrix equation of the form

$$U_L \vec{\psi}^{(t+\Delta t)} = U_R \vec{\psi}^{(t)} \quad (29)$$

with U_L, U_R complex entry sparse matrices of $(J_{q1}+1) \times (J_{q1}+1) \times \dots \times (J_{qn}+1) \times (J_{qn}+1)$ dimensions, with only $2n+1$ non-zero elements per column and such that $U_L = U_R^*$.

Finally, let us develop the shape of these matrices inductively.

The $n = 1$ case

The discretized wave-vector at each time will be a vector $\vec{\psi}^{(t)} = (\psi_0^{(t)}, \dots, \psi_J^{(t)}) \in \mathbb{C}^{J+1}$ such that, equation (24) would be

$$b_j^{(t+\Delta t)} \psi_j^{(t+\Delta t)} + a(\psi_{j-1}^{(t+\Delta t)} + \psi_{j+1}^{(t+\Delta t)}) = d_j \psi_j^{(t)} + a(\psi_{j-1}^{(t)} + \psi_{j+1}^{(t)}), \quad (30)$$

with

$$b_j := 1 + \frac{i\Delta t \hbar}{2m(\Delta q)^2} + \frac{i\Delta t}{2\hbar} V_j; \quad d_j := 1 - \frac{i\Delta t \hbar}{2m(\Delta q)^2} - \frac{i\Delta t}{2\hbar} V_j; \quad a := \frac{-i\Delta t \hbar}{4m(\Delta q)^2}. \quad (31)$$

This can be rearranged into the matrix equation (29) if U_L and U_R are the complex conjugate $(J+1) \times (J+1)$ tridiagonal matrices

$$U_L = \begin{pmatrix} b_0 & a & & & \\ a & b_1 & a & & \\ & a & b_2 & a & \\ & & \ddots & \ddots & \ddots \\ & & & a & b_{J-1} & a \\ & & & & a & b_J \end{pmatrix}; \quad U_R = \begin{pmatrix} d_0 & -a & & & \\ -a & d_1 & -a & & \\ & -a & d_2 & -a & \\ & & \ddots & \ddots & \ddots \\ & & & -a & d_{J-1} & -a \\ & & & & -a & d_J \end{pmatrix} \quad (32)$$

The $n = 2$ case

This time, the discretized wave-vector will be $\vec{\psi}^{curr} = (\psi_{00}^{curr}, \psi_{10}^{curr}, \dots, \psi_{J_1 0}^{curr}, \psi_{01}^{curr}, \psi_{11}^{curr}, \dots, \psi_{J_1 J_2}^{curr}) \in \mathbb{C}^{(J_1+1) \times (J_2+1)}$, such that equation (24) would be

$$\begin{aligned} & b_{jk}^{next} \psi_{jk}^{next} + a_1(\psi_{j-1,k}^{next} + \psi_{j+1,k}^{next}) + a_2(\psi_{j,k-1}^{next} + \psi_{j,k+1}^{next}) = \\ &= d_{jk}^{prev} \psi_{jk}^{prev} + a_1(\psi_{j-1,k}^{prev} + \psi_{j+1,k}^{prev}) + a_2(\psi_{j,k-1}^{prev} + \psi_{j,k+1}^{prev}) \end{aligned} \quad (33)$$

with

$$b_{jk} := 1 + \frac{i\Delta t \hbar}{2} \left(\frac{1}{m_1(\Delta x_1)^2} + m_2(\Delta x_2)^2 \right) + \frac{i\Delta t}{2\hbar} V_{jk}; \quad d_{jk} := b_{jk}^*; \quad a_r := \frac{-i\Delta t \hbar}{4m_r(\Delta x_r)^2}. \quad (34)$$

This can be rearranged into the matrix equation (29), if U_R, U_L are the complex $(J_1 + 1)(J_2 + 1) \times (J_1 + 1)(J_2 + 1)$ sparse matrices with a maximum of 5 non-null elements per column,

$$U_L = \left(\begin{array}{c|cc|cc|cc|cc} b_{00} & a_1 & & a_2 & & & & & \\ a_1 & b_{10} & a_1 & & a_2 & & & & \\ \ddots & \ddots & \ddots & & \ddots & & & & \\ a & b_{J_1,0} & & & & a_2 & & & \\ \hline a_2 & & b_{01} & a_1 & & a_2 & & & \\ & a_2 & a_1 & b_{11} & a_1 & & a_2 & & \\ & & \ddots & \ddots & \ddots & & \ddots & & \\ & & & a_1 & b_{J_1,1} & & a_2 & & \\ & a_2 & & & & & a_2 & & \\ & & a_2 & & & & & \ddots & \\ & & & a_2 & & & & & a_2 \\ & & & & \bullet & & & & \\ & & & & \bullet & & & & a_2 \\ & & & & \bullet & & & & \\ & & & & \bullet & & & & a_2 \\ & a_2 & & a_2 & & b_{0J_2} & a_1 & & \\ & & a_2 & & a_1 & b_{0J_2} & a_1 & & \\ & & & & \ddots & \ddots & \ddots & & \\ & & & & & a_1 & b_{1J_2} & & \end{array} \right); \quad U_R = \overline{U_L}$$

Note that U_L contains the U_L matrix we had in the $n = 1$ case, but replicated for each of the possible positions in the second dimension ($J_2 + 1$ times). We will use this observation for the generalization.

The $n=3$ and $n=N$ case

For $n = 3$, the wave-vector would be $\vec{\psi}^{curr} = (\psi_{000}^{curr}, \dots, \psi_{J_1 00}^{curr}, \psi_{010}^{curr}, \dots, \psi_{J_1 10}^{curr}, \dots, \psi_{J_1 J_2 0}^{curr}, \psi_{001}^{curr}, \dots, \psi_{J_1 J_2 1}^{curr}, \dots, \psi_{J_1 J_2 J_3}^{curr}) \in \mathbb{C}^{(J_1+1) \times (J_2+1) \times (J_3+1)}$. In this case, the matrices U_L and U_R would be conjugate $(J_1+1)(J_2+1)(J_3+1) \times (J_1+1)(J_2+1)(J_3+1)$ sparse matrices with at most 7 non-null elements per column. Drawing the whole matrix in a page is complicated, but following the “inception” we observed for the $n = 2$ case, the general pattern can be easily abstracted. U_L will contain in its diagonal a “repetition” of the $n = 2$ matrix, repeated $(J_3 + 1)$ times with two bands of a_3 coefficients crossing the diagonals that touch the vertices of the copies of 2D U_L -s, just like the a_2 did with the vertexes of the $n = 1$ sub-matrix blocks. See a graphical intuition in Figure 7.

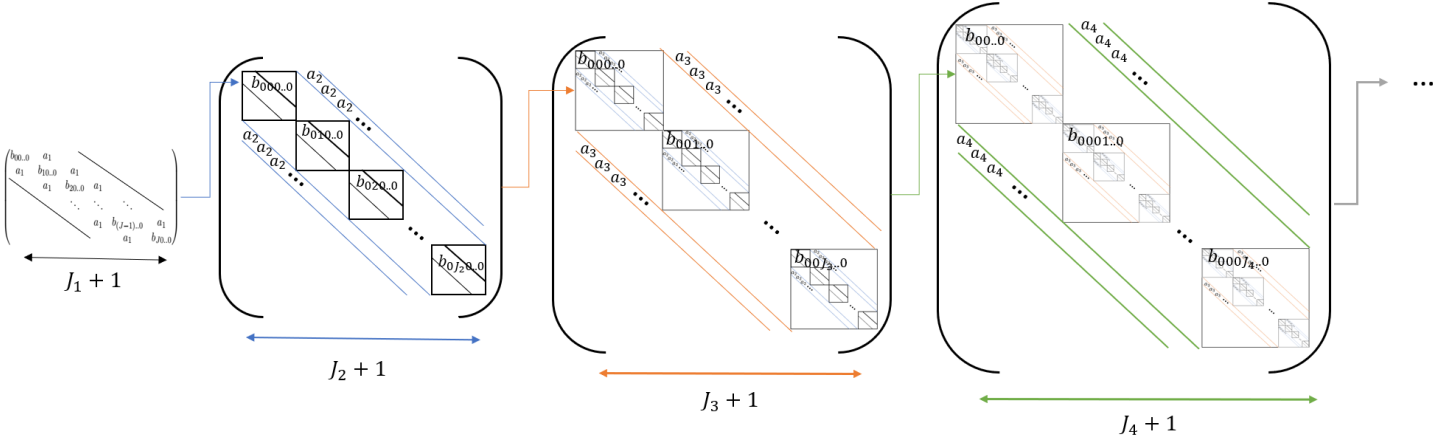


Figure 7: Schematic representation of the "fractal" construction of U_L for several dimensions. From left to right, the U_L matrix fro $n = 1, 2, 3, 4....$. With that, we can get U_R as $U_R = U_L^*$.

Generalizing this recursive construction, it is possible to define U_L and U_R for an arbitrary n in a recursive manner. Per each additional dimension $n = k + 1$, consider the U_L and U_R of the previous case $n = k$ and repeat them as many times as points considered in the new dimension ($J_{x_k} + 1$). Then add an additional index labeling each repeated block and place them as diagonal blocks of a bigger matrix. Each of these blocks will describe the time evolution of all the rest of dimensions conditioned to a particular point of the newly considered one. Finally, the a_{k+1} coefficients will be repeated diagonally tangent to the edges of the blocks of a dimension less.

With this recursive construction, one proves algorithmically that for increasing dimensions of the quantum system, the problem to be solved gets its complexity in time and space increased exponentially. This is the quantum many-body problem.

C: COMPARISON METRICS

In order to quantitatively check how close the predictions of both theories are, we need to define some comparison metrics. For this, we assume that we have at our hands the trajectories, their velocities, the density and the velocity fields, estimated from the countable Universe approach, respectively $\{\vec{x}_{CU}^\xi(t)\}_{\xi \in \sigma}, \{\vec{v}_{CU}^\xi(t)\}_{\xi \in \sigma}, \rho_{CU}(\vec{x}, t), \vec{v}_{CU}(\vec{x}, t)$; and those estimated with the SE, respectively $\{\vec{x}_{SE}^\xi(t)\}_{\xi \in \sigma}, \{\vec{v}_{SE}^\xi(t)\}_{\xi \in \sigma}, \rho_{SE}(\vec{x}, t), \vec{v}_{SE}(\vec{x}, t)$. We assume that the initial time conditions for the trajectories match in both results, such that $\vec{x}_{SE}^\xi(t_0) = \vec{x}_{CU}^\xi(t_0)$ and $\vec{v}_{SE}^\xi(t_0) = \vec{v}_{CU}^\xi(t_0)$.

C.1 Trajectory Metrics

(a) A metric reflecting the strict divergence between equally initialized trajectories,

$$\mathcal{C}_a(\{\vec{x}_{CU}^\xi(t)\}_{\xi \in \sigma}, \{\vec{x}_{SE}^\xi(t)\}_{\xi \in \sigma}) = \sum_{\xi \in \sigma} \frac{\int_{t_0}^{t_f} \|\vec{x}_{CU}^\xi(t) - \vec{x}_{SE}^\xi(t)\| dt}{|\sigma|(t_f - t_0)} \quad (35)$$

where $|\sigma|$ is the cardinality of σ (the number of simulated trajectories) and t_0, t_f are the initial and final times. As time goes on, it happens that the ξ -th CU trajectory deviates from the SE ξ -th trajectory, to the point that it might get to represent another SE trajectory. This metric is intolerant to such events.

(b) Interpolate the SE velocity field $\vec{v}_{SE}(\vec{x}, t)$ on the CU trajectories $\{\vec{x}_{CU}^\xi(t)\}_{\xi \in \sigma}$ to get $\{\vec{v}_{SE \rightarrow CU}^\xi(t)\}_{\xi \in \sigma}$, the velocities that the

CU trajectories should have according to their position but in the SE. Then compute the average divergence

$$\mathcal{C}_b(\{\vec{x}_{CU}^\xi(t)\}_{\xi \in \sigma}, \vec{v}_{SE}) = \sum_{\xi \in \sigma} \frac{\int_{t_0}^{t_f} \|\vec{v}_{CU}^\xi(t) - \vec{v}_{SE \rightarrow CU}^\xi(t)\| dt}{|\sigma|(t_f - t_0)} \quad (36)$$

This metric is more tolerant with the mixing of the trajectories.

C.2 Field Metrics

(c) The average point-wise difference of the densities

$$\mathcal{C}_c(\rho_{CU}, \rho_{SE}) = \frac{\int_{t_0}^{t_f} \int_{\Omega} |\rho_{SE}(\vec{x}, t) - \rho_{CU}(\vec{x}, t)| dt}{(t_f - t_0)|\Omega|}, \quad (37)$$

where $|\Omega|$ is the n -volume enclosed in Ω .

(d) The same for the velocities

$$\mathcal{C}_d(\vec{v}_{CU}, \vec{v}_{SE}) = \frac{\int_{t_0}^{t_f} \int_{\Omega} \|\vec{v}_{SE}(\vec{x}, t) - \vec{v}_{CU}(\vec{x}, t)\| dt}{(t_f - t_0)|\Omega|}, \quad (38)$$

which is somewhat the reciprocal of (b).

C.3 Others

Let us define the expectation of an observable using the probability density $\rho(\vec{x}, t)$ and the property field $\mathfrak{O}(\vec{x}, t)$ as

$$\langle \mathfrak{O} \rangle_\rho(t) := \int_{\Omega} \rho(\vec{x}, t) \mathfrak{O}(\vec{x}, t) dx, \quad (39)$$

and let us define the expectation using a representative ensemble $\{\vec{x}^\xi(t)\}_{\xi \in \sigma}$ following ρ together with the properties over them $\mathfrak{O}^\xi(t)$, as

$$\langle \mathfrak{O} \rangle_{trj}(t) := \sum_{\xi \in \sigma} \frac{\mathfrak{O}^\xi(t)}{|\sigma|}. \quad (40)$$

(e) The average difference between the expected position predictions using SE and MIW,

$$\mathcal{C}_e^* = \frac{\int_{t_0}^{t_f} |\langle \vec{x} \rangle_*^{SE}(t) - \langle \vec{x} \rangle_{trj}^{CU}(t)| dt}{t_f - t_0} \quad (41)$$

with $* \in \{\rho, trj\}$.

(f) The difference between the expected velocity predictions

$$\mathfrak{C}_e^* = \frac{\int_{t_0}^{t_f} \|\langle \vec{v} \rangle_*^{SE}(t) - \langle \vec{v} \rangle_{trj}^{CU}(t)\| dt}{t_f - t_0} \quad (42)$$

with $* \in \{\rho, trj\}$.

(g) For the cases in which we want to see the transmittance above a certain hyperplane $\{x_k > r\}$ with $r \in \mathbb{R}$, we use the same definitions as (39) and (40) but change Ω by $\Omega_r := \{\vec{x} \in \Omega : x_k > r\}$ and σ by $\sigma_r := \{\vec{\xi} \in \sigma : x_k^\xi(t) > r\}$. Then, $\langle 1 \rangle(t)$ will be the transmitted density above $x_k = r$, such that we can define the average discrepancy as

$$\mathfrak{C}_g^* = \frac{\int_{t_0}^{t_f} |\langle 1 \rangle_*^{SE}(t) - \langle 1 \rangle_{trj}^{CU}(t)| dt}{t_f - t_0} \quad (43)$$

with $* \in \{\rho, trj\}$.

D: THE SAMPLING PROBLEM

Given an initial wavefunction (or equivalently, an initial probability density $\rho(\vec{x}, t_0)$ and a velocity field $\vec{v}(\vec{x}, t_0)$), special care must be taken in the sampling of the initial trajectories. The naivest way to sample them is to generate a spatial grid of points $\{x_k^{(j)}\}_{k,j}$ (following the notation in Appendix B), evaluating the probability density over it, $\rho_{(j_1, \dots, j_n)} := \rho(x_1^{(j_1)}, \dots, x_n^{(j_n)}, t_0)$, and then using the finite set $\{\rho_{(j_1, \dots, j_n)}\}_{(j_1, \dots, j_n)}$ as the relative probabilities of sampling the trajectory in one of the grid points. Any code to get samples from a finite vector of probabilities would suffice for this. For each asked sample, we would get a grid node index, indicating the trajectory position together with the initial velocity (by the same grid indices). This method has several problems though: (i) for high dimensionalities n , computational limitations will force us to use a grid with few points per axis, (ii) the number of sampled trajectories for a working MIW simulation will presumably be very high, (iii) typically, initial probability densities (e.g., Gaussian wavepackets) are localized, leaving a significant probability over a very scarce set of grid points. The three together cause that many of the initialized trajectories will be sampled at the same exact spots, giving rise to superimposed or multi-trajectories that remain together at all times.

One could naively think that these multi-trajectories are nothing different from singular trajectories, because they never split in two. However, in the MIW approach, the force exerted by a multi-trajectory on the rest of trajectories is the force due to its position but multiplied by its multiplicity. This will not produce the same dynamics as if there were no superimposed trajectories. Even if the multi-trajectory got far from the rest, it would still have a multiplied influence on them, and more importantly, the density estimation on its region would still be significant, although all its immediate locality could have been depleted. Again, naively, one could think that this is fair, because that trajectory should be able to convey its probability with it, which was high at the beginning, so why not later on? This however is an incorrect point. The probability density is **not** conserved over Bohmian trajectories in the Schrödinger Equation. In particular, if one writes the continuity equation (2) in the Lagrangian frame, one gets

$$\frac{d\rho(\vec{x}^\xi(t), t)}{dt} = -\rho(\vec{x}^\xi(t), t) \sum_{k=1}^n \frac{\partial v_k(\vec{x}, t)}{\partial x_k} \Big|_{\vec{x}=\vec{x}^\xi(t)} \quad (44)$$

showing that only if the gradient of the velocity field is zero the density is conserved along the trajectories, which does not typically happen. One can then see that the density over a trajectory dilutes or concentrates exclusively due to the divergence of the velocity field [10]. This implies for the MIW that if the locality of a trajectory gets depleted of other trajectories, its “over-representation” should also be diluted correspondingly.

The best way to avoid this problem is to use a sampling technique that does not rely on a grid, but instead, samples points \vec{x} arbitrarily in the domain of the density. One such method (that we implemented) is the well-known rejection sampling [20]. This is a stochastic sampling method that given another method to generate random numbers following a known probability density (e.g. uniformly distributed numbers), allows to sample numbers from another known (but hard to sample) density. Among the down-sides of such a method however, we have that as the dimensionality of configuration-space increases, the number of rejected samples will be each time bigger, requiring more time in average until all the desired trajectories are sampled; or the fact that the method requires an upper bound of the density we want to sample from, which is a parameter that is therefore needed along the initial wavefunction (unlike in the grid sampling technique).

E: A PHILOSOPHICAL DIGRESSION: ARE TANGENT UNIVERSES COMPATIBLE WITH OBSERVATIONS?

First, why “tangent” and not, say, “parallel”? Well, due to the existence and uniqueness theorems of ordinary differential equations, Bohmian trajectories (7) never cross each other in configuration space. Even if there are arbitrarily close Bohmian trajectories to any other, tangentially close, to the point that they can very strongly interact (just as we have seen in this work for the “discretized” case), they never cross each other. And yet, we do not refer to them as “parallel” Universes (if we consider the quantum system as the whole Universe), because the information of all the other trajectories is implicit in the dynamics of any of them. Bohmian theorists call the other possible trajectories, “the pilot-wave”, and claim that ontologically, the reason that explains the wave-particle dualism of quantum mechanics is simply that there is indeed a particle (a Universe) and a pilot-wave (guiding it). They say that one thing cannot be a wave and a particle at the same time, but two can. We here, have claimed a radically different thing, that infinite particles can behave both as particles (each of them) and as a wave (due to their ensemble interaction). That is, we postulate that the rest of possible Bohmian trajectories are actual other Universes that exist equally strongly as ours. And we claim that the MIW approach can only be understood within this interpretation.

But what would this mean observationally? Well, because under this interpretation, the particles of our same body are part of the most general quantum system, the Universe, we are trapped in one of the non-crossing trajectories, meaning we would never observe any other Universe. That is, we would observe no superpositions, no dead and alive cats simultaneously, no decayed radioactive particle and undecayed simultaneously. Only a dynamical effect of the rest of possible states in ours. And although we placed a very sensitive detector down at the electronic level, our detection screen would only detect a point-like particle. But, hey, that is just what we observe every day, both in the lab and at

home.

It turns out that taking the tangent universe interpretation seriously in philosophical grounds can be a nice existential relief in front of all the paradoxes and spooky properties of orthodox quantum mechanics. Because under this interpretation of the quantum formalism, we would be part of only one of these Universes, this would explain why we always measure particles to be point-like, although they manifest wave-like behaviour, it would explain why we have never perceived any superposition. No Schrödinger's cat paradox. But moreover, the measurement problem of quantum mechanics would also vanish. The randomness of quantum mechanics would no longer be fundamental. Instead, it would only be due to our ignorance about which is the label of our Universe. Because it is not possible to access the position of all the degrees of freedom of the Universe at a same time, the best we can do is to place an equal probability to any of the Universes in the configuration-space fluid of Universes. If so, the density of Universes would be equal to the probability density of Universes, which turns out to be the well-known Born's law. Ontologically, on the other hand, at the fabric of existance, physics would be completely deterministic and ruled by the unitary Schrödinger equation (satisfying Einstein's famous claim that God does not play dice). Then, all the non-unitary collapses of the wavefunction and the SE dynamics for systems that are smaller than the whole Unibverse (as is typically our interest), would be simply be derived as corollaries (and not postulated), following a similar procedure to the Bohmian community [6, 21]. Interestingly, one of the main criticism to the Bohmian interpretation, about where the pilot wave is, or whether it is experimentally accessible, or the one about the meaning of probability in the Universal level, would be both bypassed without any problem under the tangent Universe interpretation.